Cofactor-specific photochemical function resolved by ultrafast spectroscopy in photosynthetic reaction center crystals

Libai Huang[a,1], Nina Ponomarenko[b], Gary P. Wiederrecht[c], and David M. Tiede[b,1]

[a]Notre Dame Radiation Laboratory, University of Notre Dame, Notre Dame, IN 46556; [b]Chemical Sciences and Engineering Division, Argonne National Laboratory, Argonne, IL 60439; and [c]Center for Nanoscale Materials, Argonne National Laboratory, Argonne, IL 60439

Edited by Graham Fleming, University of California, Berkeley, CA, and approved January 25, 2012 (received for review October 13, 2011)

High-resolution mapping of cofactor-specific photochemistry in photosynthetic reaction centers (RCs) from *Rhodobacter sphaeroides* was achieved by polarization selective ultrafast spectroscopy in single crystals at cryogenic temperature. By exploiting the fixed orientation of cofactors within crystals, we isolated a single transition within the multicofactor manifold, and elucidated the site-specific photochemical functions of the cofactors associated with the symmetry-related active A and inactive B branches. Transient spectra associated with the initial excited states were found to involve a set of cofactors that differ depending upon whether the monomeric bacteriochlorophylls, $BChl_A$, $BChl_B$, or the special pair bacteriochlorophyll dimer, P, was chosen for excitation. Proceeding from these initial excited states, characteristic photochemical functions were resolved. Specifically, our measurements provide direct evidence for an alternative charge separation pathway initiated by excitation of $BChl_A$ that does not involve P*. Conversely, the initial excited state produced by excitation of $BChl_B$ was found to decay by energy transfer to P. A clear sequential kinetic resolution of $BChl_A$ and the A-side bacteriopheophytin, BPh_A, in the electron transfer proceeding from P* was achieved. These experiments demonstrate the opportunity to resolve photochemical function of individual cofactors within the multicofactor RC complexes using single crystal spectroscopy.

photosynthesis | transient absorption | light-harvesting

In contrast to the diverse array of structures that have evolved for photosynthetic light-harvesting, a conserved feature of photosynthetic reaction centers (RCs) is the hexameric cofactor core that converts optical excited states to charge-separated states as the first chemical reaction in photosynthesis (1–3). Crystal structures from both oxygenic and nonoxygenic photosynthetic reaction center complexes show the hexameric cofactor core to be arranged with a pseudo twofold axis of symmetry consisting of the primary electron donor special pair (P), a dimer of (bacterio) chlorophyll molecules, and two branches, labeled A and B, that are equivalently positioned to serve as electron acceptor chains that extend across the membrane as depicted in the inset of Fig. 1 (4–6). The primary light-initiated electron transfer steps have been extensively investigated in bacterial Type II RCs and are considered to proceed from the excited singlet state P* to A side bacteriopheophytins (BPh_A) using A side bacteriochlorophyll ($BChl_A$) as a largely kinetically unresolved first electron acceptor (7–9) with the reaction directionality understood to be determined primarily by differences in local protein-site determined energetics for electron transfer along the two cofactor branches (10–12).

The above view leaves in question the role for the conserved, but nominally inactive B-side pigments. Possible complexities in primary photochemistry for the bacterial RC multicofactor core have been suggested by findings of excitation energy-dependent variation photochemical pathways (13, 14), including those that do not involve P* (15, 16) that are analogous to the primary processes identified in Photosystem I and II reaction centers in oxygenic photosynthesis.(17–20). Analysis of a broad range of spectroscopic, excitation energy transfer, and electron transfer properties based on modeling the electronic structure of RCs have led to the concept that the hexameric cofactor core should be considered as a supermolecule with a ladder of exciton states composed of various contributions from each of the individual cofactors (21–23). Further, recent 2D electronic spectroscopic studies revealed surprisingly long-lived excited-state quantum coherence between cofactors preserved by correlated protein environments in photosynthetic light-harvesting and reaction center complexes (24–29). This intercofactor electronic coherence is significant as a conduit for energy transfer that is potentially relevant to electron transfer as well. Interpigment electronic coupling has been studied by ultrafast pump-probe anisotropy spectroscopy in solution (28, 30, 31). Interpigment couplings in these measurements are detected through delocalized excited-state absorption changes, including coherent wave-packet motion, (25, 31–33) and by polarization studies that resolve transition moment anisotropies that deviate from the individual molecular reference frames (30, 31, 34, 35). Limitations for photo-selection spectroscopy arise from the inability of excitation pulses to selectively isolate a single transition in regions of spectral congestion.

Ultrafast transient absorption spectroscopy on single crystals of the bacterial RC (36) and a cyanobacterial cytochrome b_6/f (37) has been used to resolve cofactor photochemistry directly related to crystal coordinate data. Further, in contrast to photo-selection spectroscopy in solution, polarized ultrafast spectroscopy on single crystals offers the additional opportunity to exploit the fixed orientation of cofactors for both pump and probe measurements. For example, the A-and B-branch cofactors have different projections along the unit cell axes of orthorhombic crystals, allowing both pump and probe to isolate individual transitions of the normally symmetry degenerate pairs (36).

In this paper, we report on polarization selective femtosecond transient absorption spectroscopy of cryogenically cooled (100 K) single reaction center crystals from *Rhodobacter sphaeroides*. Combinations of pump wavelength and polarization were used to selectively excite optical transitions of P_- (the lower exciton state of P), $BChl_A$ and $BChl_B$ in the Q_y spectral region. By isolating a single transition within the cofactor manifold at a time, we are able to map cofactor-specific charge separation pathways. This approach provides unique opportunities to exploit the fixed orientation of cofactors within crystals to achieve site-specific excitation and detection of cofactors, and to elucidate photochemical

Author contributions: L.H., G.P.W., and D.M.T. designed research; L.H. and N.P. performed research; G.P.W. contributed new reagents/analytic tools; L.H. and D.M.T. analyzed data; and L.H. and D.M.T. wrote the paper.

The authors declare no conflict of interest.

This article is a PNAS Direct Submission.

[1]To whom correspondence may be addressed. E-mail: lhuang2@nd.edu or tiede@anl.gov.

This article contains supporting information online at www.pnas.org/lookup/suppl/doi:10.1073/pnas.1116862109/-/DCSupplemental.

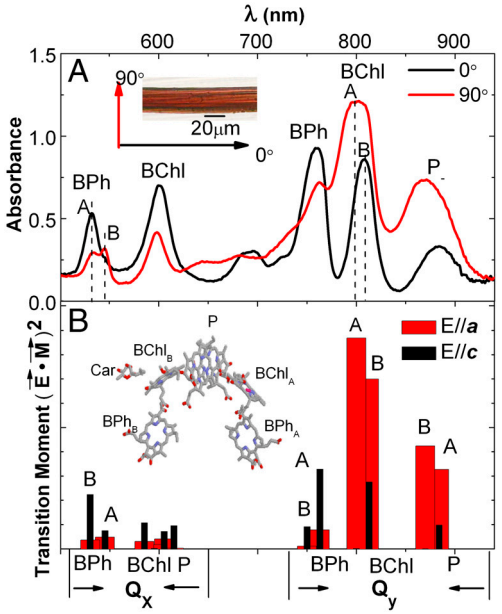

Fig. 1. Polarized ground state optical absorption for a single *R. sphaeroides* R26 RC crystal ($P2_12_12_1$) at 100 K. Part (*A*) shows ground state absorption spectra measured with light polarized perpendicular (90°) and parallel (0°) to the long axis of the crystal. The inset in part (*A*) shows a representative photograph of the wild-type (WT) crystals used in the experiments. The (*B*) box shows transition moment projections along the crystal ***a*** (red) and ***c*** (black) axes, respectively. The inset in (*B*) illustrates the arrangement of the cofactors in RCs. Letters A and B denote branches in RC molecule.

functions of cofactors associated with the active A branch and inactive B branch in bacterial RCs.

Results

Ground state polarized absorption spectra for cryogenically cooled (100 K) crystals are shown in Fig. 1. Extinction coefficient weighted projections for each of the RC cofactor optical transitions along the ***a*** and ***c*** crystal axes are plotted with wavelength positions according to cofactor peak assignments (23, 38, 39) in Fig. 1*B*. Magnitudes for polarized optical absorption for the RC $P2_12_12_1$ unit cell were calculated from the transition moment, the polarized light electric field, and unit vectors as described previously (36). Absorption spectra were measured with light polarized either parallel (0°) or perpendicular (90°) to the long axis of the needle-shaped crystal (inset of Fig. 1*A*). X-ray alignment measurements show that the unit cell directions lie parallel to the crystal axes (40, 41). The agreement between the measured spectra and calculated transition moment projections allows the experimental 0° and 90° directions to be identified as lying along the 4RCR crystal unit cell ***c*** and ***a*** axes, respectively (36). Further details are provided in the *SI Text*.

As illustrated in Fig. 1*A*, the ground state polarized absorption spectra show pronounced variation in both absorption peak positions and amplitudes as the polarization angle for the measuring beam is rotated from 0° to 90°. For instance, the BPh Q_x peak at 530 nm reflects predominate contribution from BPh_B at 0° polarization, while the spectrum recorded with 90° polarized light shows split absorption bands corresponding to the BPh_B (530 nm) and BPh_A (545 nm) contributions, respectively. The spectrum recorded with 90° polarized light shows a peak centered at 800 nm that reflects the greater contribution of $BChl_A$. With 0° polarized light, the BChl peak absorption shifts to 810 nm, and based on the agreement with transition moment projection onto the crystal axes can be understood to be contributed mainly by $BChl_B$. Note that the upper energy exciton component of P_+ is known to have an absorption band that overlaps with $BChl_B$ around 810 nm but with only approximately 1/3 of the oscillation strength of the $BChl_B$ (42). The red-most absorption band arises from the lower energy exciton component of P, P_- (43). Models have taken into account the effects of coupling between all of the cofactor transition dipoles within the RC and charge transfer states between BChl comprising P.(22, 23). The polarized spectra recorded for P_- is found to have a strong preferential absorption with 90° polarized light. The absorption spectra shown in Fig. 1 are from a R26 crystal. The experiments described below are performed on wild-type (WT) crystals. The ground state dichroism is similar for R26 and WT crystals and the absorption spectra for a typical WT crystal are shown in Fig. S1*A*.

Based on the ground state dichroism discussed above, the polarization angle can be combined with wavelength to selectively excite and probe otherwise degenerate optical transitions of cofactors associated with the A and B branches (36). The opportunity to resolve cofactor-specific photochemical function by polarization selective transient spectroscopy measurements in single crystals is illustrated in Fig. 2. Three pump wavelength and polarization combinations were utilized to selectively excite the Q_y transition of P_- (900 nm, bandwidth approximately 28 nm, 90° polarization Fig. 2*A*), $BChl_A$ (790 nm, bandwidth approximately 20 nm, 90°polarization, Fig. 2*B*), and $BChl_B$ (824 nm, bandwidth approximately 23 nm, 0° polarization, Fig. 2*C*). The spectra of the pump pulses are shown in Fig. S1*B*. The white-light probe polarization was set to be either 90° (top graphs) or 0° (bottom graphs). Probing at 0° and 90° produced dramatically different spectra, demonstrating the ability to selectively probe different transitions in the manifold (36). Specifically, bleaching of the Q_x transition of BPh_A around 545 nm is observed almost exclusively with the 90° polarized probe. This observation is consistent with the experimental polarized ground state spectra, in that the BPh_A Q_x transition moment is aligned preferentially with the ***a*** axis. Transient spectra for each pump and probe combination are compared at four delay times in Fig. 2. The corresponding 2D graphs illustrating the full time progression for the transient absorption measured during the experimental time frame are shown in Fig. S2.

The initial transient states and progression of subsequent energy and electron transfer events show clear differences that depend upon the cofactor-specific excitation. The position of the initial BChl Q_x transition bleach near 600 nm accompanying excitation in the near-IR Q_y region was found to shift characteristically depending upon the BChl cofactor selected for photoexcitation. For example, when the Q_y transition of P_- is selectively excited, the initial bleaching is at 604 nm corresponding to the Q_x transition of P (Fig. 2*A*, 0.1 ps trace). We note that the P Q_x transition makes only a minor projection onto the crystal axis probe by the 90° probe orientation. The bottom graph of Fig. 2*A* shows the transient spectrum measured with 0° probe following 900 nm, 90° excitation, and the larger P Q_x bleaching. When $BChl_A$ is selectively excited, the initial bleaching occurs at 595 nm consistent with the Q_x transition of $BChl_A$ (Fig. 2*B*, 0.1 ps trace). Finally, an initial bleaching at 609 nm is observed with an excitation wavelength of 824 nm and a polarization at 0° (Fig. 2*C*, 0.1 ps trace). This position is different from the Q_x transition of P at 604 nm and if the P_+ transition were excited, one would expect the bleach to be at 604 nm. Therefore, we assign the bleach observed at 609 nm to the Q_x transition of $BChl_B$. Even though there is significant spectral overlap between Q_y transition of $BChl_B$ and P_+ state, the instantaneous bleach at 609 nm instead of at 604 nm indicates that the pump wavelength of 824 nm at 0° polarization excites mostly the Q_y transition of $BChl_B$ instead of P_+.

In addition to the resolution of BChl Q_x bleaching components, the earliest transient spectra show initial excite states to involve a set of cofactors that differ depending upon whether $BChl_A$, $BChl_B$, or P_- was chosen for excitation. For example, with the selective excitation of P_-, a partial absorption decrease of the BPh_A Q_x transition at 545 nm is seen in the transient spectrum

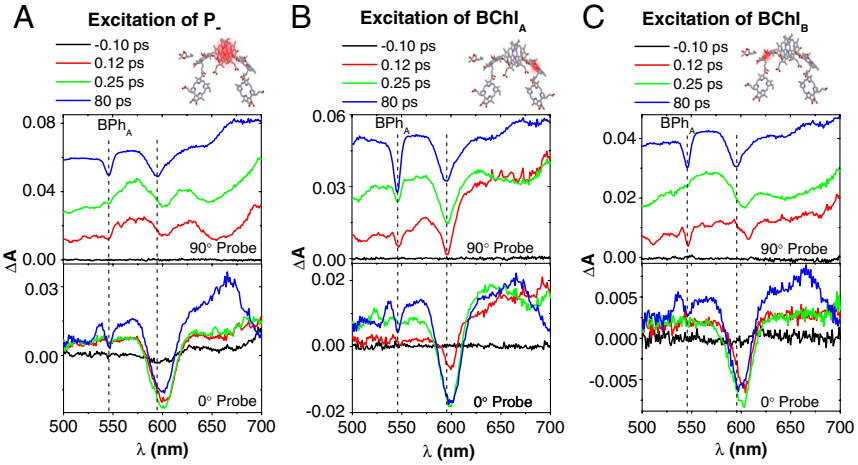

Fig. 2. Pump wavelength-dependent patterns of transient optical absorption changes in a single *Rb. sphaeroides*-wt crystal at 100 K. The pump is adjusted to 900 nm (90°), 790 nm (90°), and 824 nm (0°), in boxes (*A, B,* and *C*), to selectively pump Q_y optical transitions of P_-, $BChl_A$ and $BChl_B$, respectively. The top spectra are for probing at 90° with respect to the crystal c axis and the spectra are offset for clarity. The vertical lines are placed at 545 and 595 nm. The bottom spectra are the spectra for probing at 0°.

recorded with a 100 fs delay (Fig. 2*A*). This instantaneous BPh_A bleach recovers, and by 200 fs the transient spectrum reflects a localized P* state. When $BChl_A$ is selectively excited by the 790 nm pump, a larger magnitude of bleach at 545 nm is observed to coincide with excitation. In addition to the instantaneous bleach of BPh_A, bleaching of carotenoid (Car) transition at 510 nm is also evident, suggesting that the initial excited-state perturbation extents to the Car cofactor. With $BChl_B$ excitation by pump wavelength of 824 nm (Fig. 2*C*), instantaneous bleaching of both the BPh_A (545 nm) and Car (510 nm) cofactors is also observed. Remarkably, no involvement of BPh_B is observed upon excitation of any of the BChls, even the adjacent $BChl_B$. A small absorption loss at 530 nm is observed in the 100 fs transient spectra upon $BChl_A$ and $BChl_B$ excitation (e.g., Fig. 2 *B* and *C*) that corresponds to the position of the BPh_B Q_x absorption. However this feature is only detected with 90°, but not 0° probe polarization, Fig. 2. This polarization pattern matches that measured for the BPh_A Q_x, in the ground state spectrum, and is the opposite of that measured and predicted from the crystal coordinates for the BPh_B Q_x direction, Fig. 1.

Proceeding from these different initial excited states, distinguishable photochemical pathways are also resolved. When P_- (Fig. 2*A*) or $BChl_B$ (Fig. 2*C*) are selectively excited, the initial excited states that include different amounts of BPh_A and Car contributions, relax in 250 fs to have characteristics of a localized P*. In both cases, the P* state in turn evolves to the $P^+BPh_A^-$ state, marked by characteristic BPh_A and $BChl_A$ Q_x bleaching at 545 nm and 595 nm, respectively and an absorption of BPh_A^- at 670 nm. In contrast, when $BChl_A$ is excited, the initial BPh_A Q_x bleach does not recover fully; i.e., the bleaching at 545 nm persists at 0.25 ps (Fig. 2*B*, 90° probe 0.25 ps trace), suggesting formation of a possible initial $BChl_A^+BPh_A^-$ charge-separated state that forms directly, and does not evolve from P*. This interpretation is supported by the companion 0° probe spectrum (Fig. 2*B*, 0° probe), which measures the broad 650–700 nm bacteriochlorin anion absorption band at 0.25 ps (44). The absorption band at 650–700 nm at early delay time (0.12 ps and 0.25 ps traces) is broader than at 80 ps (Fig. 2*B*, 0° probe), which may reflect the biradical $BChl_A^+BPh_A^-$ charge-transfer state formed initially upon $BChl_A$ excitation. In contrast, upon excitation of either $BChl_B$ or P_- , a BPh anion absorption band is not observed until charge separation is completed and the P^+ BPh_A^- state is formed.

Fig. 3 shows the single-wavelength kinetics of the BPh_A Q_x transition (545 nm – 540 nm, 90° probe), taken from the data shown in Fig. 2, and measured following selective excitation of P_-, $BChl_A$, and $BChl_B$, that also reflect the site-specific charge separation pathways. At the earliest observable time (approximately 100 fs), a dip with a width of the time resolution of the experiments (approximately 150 fs) is present in all three decay curves corresponding to the instantaneous bleach observed in the spectra. The magnitude of initial BPh_A transient is 10%, 45%, and 85% of the total absorption change following excitation of P_-, $BChl_A$, and $BChl_B$, respectively. The dynamics after the initial

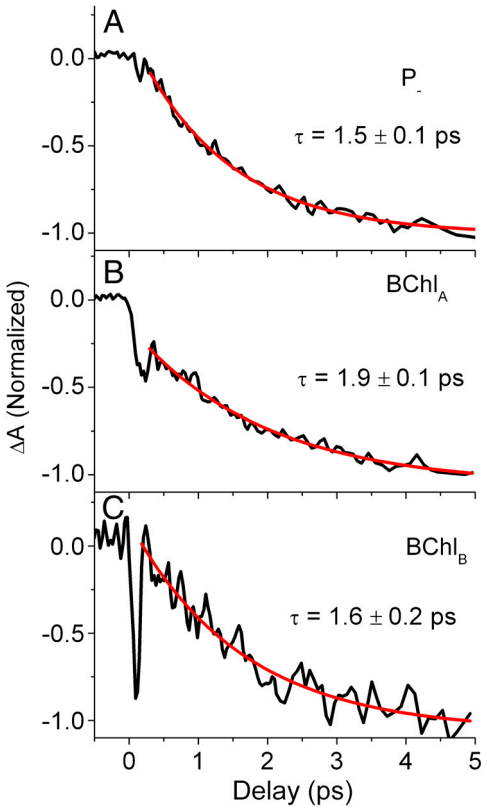

Fig. 3. Pump wavelength-dependent kinetics for the BPh_A Q_x absorption (545 nm – 540 nm) in the same *Rb. spheroides*-wt crystal as in Fig. 2. The pump was adjusted to selectively excite different RC optical transitions P- (*A*), $BChl_A$ (*B*) and $BChl_B$ (*C*). The crystal temperature was 100 K. The red lines show single exponential decay fits.

bleach are fitted with a single exponential function. When P and $BChl_B$ are selectively excited, the initial BPh_A bleach fully recovers (i.e., ΔA recovers to 0 at approximately 0.25 ps) to a P* state that subsequently decays with a time constant of approximately 1.5 ps to the $P^+BPh_A^-$ state. When $BChl_A$ is selectively excited, the initial BPh_A bleach does not recover fully (i.e., ΔA does not recover to 0), which is attributed to a mixture of $BChl_A^+BPh_A^-$ and P* states. The formation of $P^+BPh_A^-$ following these excited states is fitted with a time constant of 1.9 ± 0.1 ps.

The resolution of $BChl_A^-$ as an intermediate in the electron transfer from P* to BPh_A is also resolved in these measurements. Although resolvable in the spectra shown above, this is most clearly illustrated with a crystal that exhibited a blue shift of the $BChl_A$ Q_x peak that allowed a very clear resolution of transient function shown in, Fig. S3. With excitation of P_, the initial BChl Q_x bleach shows a single band with a peak at 604 nm associated with P*. During the subsequent electron transfer to form $P^+BPh_A^-$, an additional bleaching band builds in at 590 nm resulting in a final double peaked BChl Q_x absorption decrease, Fig. S3. The individual contributions of $BChl_A$ and BPh_A can be tracked, in difference transient spectra using the 150 fs P* as a reference spectrum, Fig. 4*A*, and corresponding single wavelength kinetics are plotted in Fig. 4*B*. The 2.2 ± 0.2 ps single exponential bleaching kinetics associated with BPh_A reduction in this crystal lag behind the bleaching of $BChl_A$, which shows biexponential kinetics with decay times of 0.9 ± 0.2 ps and 2.3 ± 0.8 ps, as described Fig. 4. Similar lag time of approximately 0.9 ps for reduction of BPh_A compared to that of $BChl_A$ is also found from difference transient spectra obtained for the crystal shown in Fig. 2, plotted in Fig. S4. We note that many experimental parameters can cause shifts in the absorption

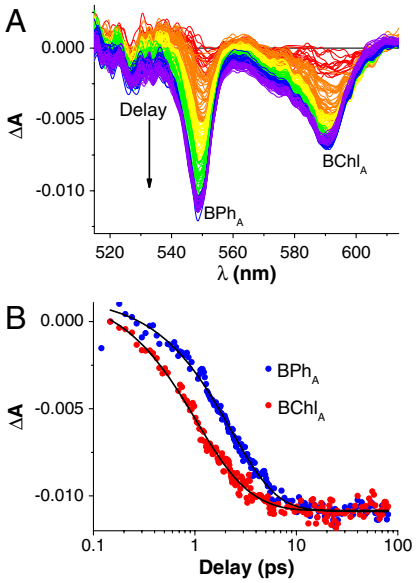

Fig. 4. Difference transient absorption spectra following formation of P*. Part (*A*) shows difference transient spectra recorded with delays from 150 fs to 80 ps, and following subtraction of the spectrum recorded with a 150 fs delay from the pump pulse. This subtraction removes contributions of ground state bleaching of P and highlights the time-progression of the BPh and BChl Q_X transient components. Part (*B*) shows single wavelength BPh_A and $BChl_A$ Q_X transient kinetics measured at 548 nm and 590 nm, respectively. The 590 nm transient was normalized to match the 548 nm amplitude. The BPh_A 548 nm kinetics were fit (solid line) using a single exponential 2.2 ± 0.2 ps decay. The $BChl_A$ 590 nm kinetics were fit (solid line) using a biexponential with 0.9 ± 0.2 ps and 2.3 ± 0.8 ps decay times corresponding amplitudes of 0.0085 ± 0.002 and 0.004 ± 0.003, respectively. Excitation was provided by 890 nm pump pulse, and both pump and probe with 90° polarized, using the transient spectra shown in Fig. S3.

peaks for the RC cofactors (45, 46). In the case of the crystal used in Fig. 4, these perturbations allowed the transient kinetics for $BChl_A$ to be more readily recognized, but comparable kinetics are observed in crystals without these perturbations, Fig. S4.

As shown here, polarization selective single crystal spectroscopy offers opportunities to resolve photochemical pathways within multicofactor photosynthetic complexes. For comparison, Fig. S5 provides an example of comparable wavelength selected excitation of detergent solubilized RCs in solution. A more complete analysis has been carried out earlier by van Grondelle and coworkers demonstrating charge-separation that did not initiate from P* (15, 16). Overall the transient absorption spectra and lifetimes measured in solution agree with those of single RC crystals, implying that the photochemical pathways are retained upon RC crystallization. The cofactor spacing between RCs within the crystal unit cell is greater than 70 Å, and crystallographic packing is unlikely to alter primary photochemistry. Spectra recorded with 0.1 ps delay show initial excited-state spectra that include contributions from BPh_A and the carotenoid cofactors, along with those of the BChl or P cofactors used for excitation. The initial excited-state spectra relax to a more localized on P* by 0.25 ps. However, because of the absence of dichroic selection, 790 nm femtosecond pump pulses excite both $BChl_A$ and $BChl_B$. The responses of $BChl_A$ and $BChl_B$ are convoluted, and the different photochemical functions of $BChl_A$ and $BChl_B$ are not readily resolved.

Discussion

Nature of the Initial Excited-States. The instantaneous bleach of BPh upon excitation of BChl has been observed previously in decay associated spectral analysis of the spectra of RC solution (47). Here we are able to observe directly from the raw data of single crystal spectroscopy, and further discriminate between the involvement of BPh_A as part of a charge-transfer state created by excitation of $BChl_A$, and the different involvement of BPh_A as part of an excited state produced by excitation of either $BChl_B$ or P.

The involvement of multiple cofactors upon single cofactor excitation can possibly be explained by strongly correlated electronic levels, possibly including charge-transfer mixing, among the individual cofactors in the RC (21, 28). Long-lived electronic coherence between the excited states of BPh and BChl was observed recently with 2-color photon echo experiments and was attributed to strong correlation between the protein-induced fluctuations in the transition energy levels of BChl and BPh (28). Electronic coherence between the cofactors allows the excitation to move coherently in space, enabling excited populations moving between different cofactors (24–29). Based on the observation of electronic coherence is much longer lived at low temperature (28), the fact that we observe multicofactor transitions in the initial excited states only at cryogenic temperature suggests that electronic coherence might play an important role. We also observe instantaneous bleaching of Car upon excitation of BChls and P, indicating Car participates in excitation energy transfer in the RC manifold. This observation is in accordance with the recent study of PSII reaction centers in which Car was suggested to act as an electronic coupling bridge and enhance energy transfer from the antenna to the reaction centers (48).

A possible alternative mechanism to explain the instantaneous bleaching of BPh_A and Car cofactors coupled to BChl excitation is through electrochromic Stark effects (49), associated with charge-transfer dipole character of initial BChl excited states. However, a Stark effect alone cannot satisfactorily explain our observations for two reasons. First, the Stark effect for an internal electric field would typically be expected to produce transient spectra with a derivative band shape, (50) but neither the instantaneous BPh_A nor Car transient bands appear to have such shapes. Secondly, a comparison of BPh_A and BPh_B Q_x directions shows that both cofactors have comparable alignments with

respect to possible excited charge-transfer state directions, Table S1, Fig. S6. Measurements using internal and external electric fields show that the B-side cofactors have a markedly enhanced electrochromic response, indicative of a dielectric asymmetry in the RC (49). We find that the opposite effect, that only BPh_A, and not BPh_B, response to BChl initial excited states.

These considerations suggest that the instantaneous bleach of multiple cofactor transitions upon single cofactor excitation of $BChl_{A,B}$ and P is most likely due to electronic coupling between the cofactor and not due to Stark effect. The lack of an involvement of the inactive BPh_B with the initial excited state formed upon excitation of $BChl_A$, $BChl_B$, or P implies an inherent asymmetry in electronic coupling between cofactors. Mutagenesis experiments have shown that directional electron transfer in RCs is largely determined by protein-tuned energies of the cofactor molecular orbitals (10, 12). Such energy level tuning can be expected to regulate the magnitudes of exciton, charge transfer, and coherent couplings between cofactors.

Photochemistry Initiated from P. Following excitation of P, the consensus view is that $BChl_A$ functions as the initial electron acceptor for P*, forming the $P^+BChl_A^-$ transient state with a 3 ps risetime (room temperature), but is rapidly converted by electron transfer to BPh_A with a 0.9 ps time constant (7). However the overlap of the ground and excited-state optical absorptions of the cofactors has posed challenges for easy verification of this reaction scheme. The spectral resolution offered by polarized transient spectroscopy on crystals shown here provides a very clear resolution of biphasic transients of the $BChl_A$ cofactor prior to BPh_A reduction. Pathway 1 in Scheme 1 summarizes the photochemistry initiated from P. These results are consistent with the kinetic scheme in which $BChl_A$ functions as the initial electron acceptor (7), but also with a more complex function discussed below.

Photochemistry Initiated from $BChl_A$ and $BChl_B$. While selective excitation of $BChl_B$ was found to create a delocalized excited state that uniformly decayed (<200 fs) to form a localized excited state on P as described above (pathway 2 in Scheme 1), more complex, dual photochemical pathways were found to accompany $BChl_A$ excitation (pathways 3a and 3b in Scheme 1). With up to 50% yield, $BChl_A$ excitation was seen to create an initial charge-separated state, $BChl_A^+BPh_A^-$, that did not evolve from P*, that persists, apparently decaying by hole transfer to form $P^+BPh_A^-$ (Pathway 3b). We note that 650 nm −670 nm BPh "anion band" absorption for this initial state differs from that detected during the transient $P^+BPh_A^-$ state, possibly a reflection of the coupled biradical natural of this initial charge-separated state. The remaining portion of the $BChl_A$ excitation appeared to decay to create P*, from which sequential electron transfer to BPh_A occurs with approximately 2 ps time constant. The presence of dual pathways suggests heterogeneity in the coupling of $BChl_A$ and BPh_A that might add complexity to the sequential electron transfer pathway.

$$P \xrightarrow{h\nu} [PBPh_A]^* \xrightarrow{<200\,fs} P^* \xrightarrow{0.9\,ps} P^+BChl_A^- \xrightarrow{2\,ps} P^+BPh_A^- \quad (1)$$

$$BChl_B \xrightarrow{h\nu} [BChl_BBPh_ACar]^* \xrightarrow{<200\,fs} P^* \xrightarrow{0.9\,ps} P^+BChl_A^- \xrightarrow{2\,ps} P^+BPh_A^- \quad (2)$$

$$BChl_A \xrightarrow{h\nu} [BChl_ABPh_ACar]^* \xrightarrow{\sim 50\%} P^* \xrightarrow{0.9\,ps} P^+BChl_A^- \xrightarrow{2\,ps} P^+BPh_A^- \quad (3a)$$

$$[BChl_ABPh_ACar]^* \xrightarrow{\sim 50\%} BChl_A^+BPh_A^- \xrightarrow{2\,ps} P^+BPh_A^- \quad (3b)$$

Scheme 1. Cofactor-specific charge separation pathways revealed by single crystal spectroscopy. The brackets list the combination of cofactor optical transitions observed for the different initial excited-states, but not the levels of their contributions.

A component of primary charge separation occurring within the $BChl_ABPh_A$ pair that does not evolve from P* was suggested previously based on decay associated spectral analysis of transients recoded from solutions at low temperature (15, 16). However, the broadness of ultrafast pump pulses and overlap of the $BChl_A$ and $BChl_B$ absorptions prevents exclusive cofactor excitation. The polarization selective spectroscopy in single crystals shown here resolves these cofactor-specific pathways with greater precision, and allows direct resolution of cofactor-specific photochemistry in the polarized transient spectra. The confirmation of alternative photochemical pathways in the bacterial RC, including those that do not involve P, provides a relevant model system for comparative analysis of photochemistry in RCs from oxygenic photosynthesis.

Single crystal ultrafast transient spectroscopy is shown to provide a means to deepen our understanding of the photophysical function of the multicofactor RC core, and establish the foundation for extending this approach to probe energy and electron transfer pathways in RC-light harvesting, PSI, PSII crystalline complexes.

Materials and Methods

Details regarding preparation of reaction center crystals, sample preparation for low temperature optical measurements, ground state absorption and transient absorption spectroscopies are presented in *SI Text*.

ACKNOWLEDGMENTS. The authors gratefully acknowledge discussions with Dr. O. Kokhan on kinetic fitting using sequential electron transfer schemes that were not presented in the manuscript. L.H. was supported by the Division of Chemical Sciences, Geosciences and Biosciences, Office of Basic Energy Sciences of the Department of Energy through Grant DE-FC02-04ER15533. N.P. and D.M.T. were supported by the Division of Chemical Sciences, Geosciences, and Biosciences, Office of Basic Energy Sciences of the Department of Energy under Contract DE-AC02-06CH11357. Use of the Center for Nanoscale Materials was supported by the Department of Energy, Office of Science, Office of Basic Energy Sciences, under Contract No. DE-AC02-06CH11357. This publication is contribution No. NDRL 4893 from the Notre Dame Radiation Laboratory.

1. Kern J, Renger G (2007) Photosystem II: Structure and mechanism of the water: plastoquinone oxidoreductase. *Photosynth Res* 94:183–202.
2. Sadekar S, Raymond J, Blankenship RE (2006) Conservation of distantly related membrane proteins: photosynthetic reaction centers share a common structural core. *Mol Bio Evol* 23:2001–2007.
3. Amunts A, Nelson N (2009) Plant photosystem I design in the light of evolution. *Structure* 17:637–650.
4. Deisenhofer J, Epp O, Miki K, Huber R, Michel H (1984) X-ray structure analysis of a membrane protein complex Electron density map at 3 A resolution and a model of the chromophores of the photosynthetic reaction center from Rhodopseudomonas viridis. *J Mol Bio* 180:385–398.
5. Jordan P, et al. (2001) Three-dimensional structure of cyanobacterial photosystem I at 2.5 angstrom resolution. *Nature* 411:909–917.
6. Zouni A, et al. (2001) Crystal structure of photosystem II from Synechococcus elongatus at 3.8 angstrom resolution. *Nature* 409:739–743.
7. Zinth W, Wachtveitl J (2005) The first picoseconds in bacterial photosynthesis—Ultrafast electron transfer for the efficient conversion of light energy. *Physical Chemistry Chemical Physics* 6:871–880.
8. Kirmaier C, Holten D (1991) An assessment of the mechanism of initial electron-transfer in bacterial reaction centers. *Biochemistry* 30:609–613.
9. Blankenship R (2002) *Molecular mechanisms of photosynthesis* (Blackwell Science, London).
10. Heller BA, Holten D, Kirmaier C (1995) Control of electron-transfer between the L-side and M-side of photosynthetic reaction centers. *Science* 269:940–945.
11. Haffa A, et al. (2003) High yield of long-lived B-side charge separation at room temperature in mutant bacterial reaction centers. *J Phys Chem B* 107:12503–12510.
12. Kirmaier C, Bautista J, Laible P, Hanson D, Holten D (2005) Probing the contribution of electronic coupling to the directionality of electron transfer in photosynthetic reaction centers. *J Phys Chem B* 109:24160–24172.
13. Lin S, Katilius E, Haffa A, Taguchi A, Woodbury N (2001) Blue light drives B-side electron transfer in bacterial photosynthetic reaction centers. *Biochemistry* 40:13767–13773.
14. Xin Y, Lin S, Blankenship RE (2007) Femtosecond spectroscopy of the primary charge separation in reaction centers of chloroflexus aurantiacus with selective excitation in the Q(Y) and soret bands. *J Phys Chem A* 111:9367–9373.

15. van Brederode M, van Mourik F, van Stokkum I, Jones M, van Grondelle R (1999) Multiple pathways for ultrafast transduction of light energy in the photosynthetic reaction center of Rhodobacter sphaeroides. *Proc Natl Acad Sci USA* 96:2054–2059.
16. van Brederode M, Van Grondelle R (1999) New and unexpected routes for ultrafast electron transfer in photosynthetic reaction centers. *FEBS Letts* 455:1–7.
17. Holzwarth AR, et al. (2006) Kinetics and mechanism of electron transfer in intact photosystem II and in the isolated reaction center: Pheophytin is the primary electron acceptor. *Proc Natl Acad Sci USA* 103:6895–6900.
18. Novoderezhkin VI, Romero E, Dekker JP, Van Grondelle R (2011) Multiple charge-separation pathways in photosystem ii: modeling of transient absorption kinetics. *Physical Chemistry Chemical Physics* 12:681–688.
19. Myers JA, et al. (2010) Two-dimensional electronic spectroscopy of the D1-D2-cyt b559 photosystem II reaction center complex. *J Phys Chem Lett* 1:2774–2780.
20. Muller MG, Slavov C, Luthra R, Redding KE, Holzwarth AR (2010) Independent initiation of primary electron transfer in the two branches of the photosystem I reaction center. *Proc Natl Acad Sci USA* 107:4123–4128.
21. Parkinson DY, Lee H, Fleming GR (2007) Measuring electronic coupling in the reaction center of purple photosynthetic bacteria by two-color, three-pulse photon echo peak shift spectroscopy. *J Phys Chem B* 111:7449–7456.
22. Warshel A, Parson W (1987) Spectroscopic properties of photosynthetic reaction centers .1. theory. *J Am Chem Soc* 109:6143–6152.
23. Parson W, Warshel A (1987) Spectroscopic properties of photosynthetic reaction centers .2. application of the theory to *Rhodopseudomonas-viridis*. *J Am Chem Soc* 109:6152–6163.
24. Novoderezhkin V, Yakovlev A, Van Grondelle R, Shuvalov V (2004) Coherent nuclear and electronic dynamics in primary charge separation in photosynthetic reaction centers: A redfield theory approach. *J Phys Chem B* 108:7445–7457.
25. Yakovlev A, et al. (2005) Primary charge separation between P* and BA: electron-transfer pathways in native and mutant GM203L bacterial reaction centers. *Chem Phys* 319:297–307.
26. Brixner T, et al. (2005) Two-dimensional spectroscopy of electronic couplings in photosynthesis. *Nature* 434:625–628.
27. Engel GS, et al. (2007) Evidence for wavelike energy transfer through quantum coherence in photosynthetic systems. *Nature* 446:782–786.
28. Lee H, Cheng Y-C, Fleming GR (2007) Coherence dynamics in photosynthesis: protein protection of excitonic coherence. *Science* 316:1462–1465.
29. Read EL, Lee H, Fleming GR (2009) Photon echo studies of photosynthetic light harvesting. *Photosynth Res* 101:233–243.
30. Jonas D, Lang M, Nagasawa Y, Joo T, Fleming G (1996) Pump-probe polarization anisotropy study of femtosecond energy transfer within the photosynthetic reaction center of Rhodobacter sphaeroides R26. *J Phys Chem* 100:12660–12673.
31. Haran G, Wynne K, Moser C, Dutton P, Hochstrasser R (1996) Level mixing and energy redistribution in bacterial photosynthetic reaction centers. *J Phys Chem* 100:5562–5569.
32. Vos MH, Breton J, Martin JL (1997) Electronic energy transfer within the hexamer cofactor system of bacterial reaction centers. *J Phys Chem B* 101:9820–9832.
33. Vos MH, Rappaport F, Lambry JC, Breton J, Martin JL (1993) Visualization of coherent nuclear motion in a membrane-protein by femtosecond spectroscopy. *Nature* 363:320–325.
34. King BA, McAnaney TB, Alex deWinter a, Boxer SG (2000) Excited state energy transfer pathways in photosynthetic reaction centers. 3. ultrafast emission from the monomeric bacteriochlorophylls. *J Phys Chem B* 104:8895–8902.
35. Klenina I, Borovykh I, Shkuropatov AY, Gast P, Proskuryakov I (2003) Orientation of the Qy optical transition moment of bacteriopheophytin in Rhodobacter sphaeroides reaction centers. *Chem Phys* 294:451–458.
36. Huang L, et al. (2008) Correlating ultrafast function with structure in single crystals of the photosynthetic reaction center. *Biochemistry* 47:11387–11389.
37. Dashdorj N, Yamashita E, Schaibley J, Cramer W, Savikhin S (2007) Ultrafast optical pump-probe studies of the cytochrome b6f complex in solution and crystalline States. *J Phys Chem B* 111:14405–14410.
38. Breton J (1985) Orientation of the chromophores in the reactioncenter of *Rhodopseudomonas viridis*. Comparison of low-tempereture linear dichroism spectra with a model derived from X-ray crystallography. *Biochim Biophys Acta* 810:235–245.
39. Kirmaier C, Holten D (1987) Primary photochemistry of reaction centers from photosyntheic purple bacteria. *Photosynth Res* 13:225–260.
40. Chang C-H, Schiffer M, Tiede DM, Smith U, Norris JR (1985) Characterization of bacterial photosynthetic reaction center crystals from *Rhodopseudomonas sphaeroides* R-26 by X-ray diffraction. *J Mol Biol* 186:201–203.
41. Chang C-H, et al. (1986) Structure of *Rhodopseudomonas sphaeroides* R-26 reaction center. *FEBS Letts* 205:82–86.
42. Jordanides X, Scholes G, Fleming G (2001) The mechanism of energy transfer in the bacterial photosynthetic reaction center. *J Phys Chem B* 105:1652–1669.
43. Lathrop EJP, Friesner RA (1994) Simulation of optical spectra from the reaction center of Rb Sphaeroides. Effects of an internal charge-separated state of the special pair. *J Phys Chem* 98:3056–3066.
44. Fajer J, Brune DC, Davis MS, Forman A, Spaulding LD (1975) Primary charge separation in bacterial photosynthesis: oxidized chlorophylls and reduced pheophytin. *Proc Natl Acad Sci USA* 72:4956–4960.
45. Wang S, Lin S, Lin X, Woodbury NW, Allen JP (1994) Comparative study of reaction centers from purple photosynthetic bacteria: Isolation and optical spectroscopy. *Photosynth Res* 42:203–215.
46. Gast P, Hemelrijk PW, Van Gorkom HJ, Hoff AJ (1996) The association of different detergents with the photosynthetic reaction center protein of Rhodobacter sphaeroides R26 and the effects on its photochemistry. *Eur J Biochem* 239:805–809.
47. Gibasiewicz K, Pajzderska M, Karolczak J, Dobek A (2009) Excitation and electron transfer in reaction centers from Rhodobacter sphaeroides probed and analyzed globally in the 1-nanosecond temporal window from 330 to 700 nm. *Phys Chem Chem Phys* 11:10484–10493.
48. Romero E, van Stokkum IHM, Dekker JP, Van Grondelle R (2011) Ultrafast carotenoid band shifts correlated with ChlZ excited states in the photosystem II reaction center: are the carotenoids involved in energy transfer? *Phys Chem Chem Phys* 13:5573–5575.
49. Steffen MA, Lao KQ, Boxer SG (1994) Dielectric asymmetry in the photosynthetic reaction-center. *Science* 264:810–816.
50. Boxer SG (2009) Stark Realities. *J Phys Chem B* 113:2972–2983.